Extensions of Fibre Bundle Models

F. Kun[1], F. Raischel[2], R.C. Hidalgo[3], and H.J. Herrmann[2]

[1] Department of Theoretical Physics, University of Debrecen, P. O. Box: 5, 4010 Debrecen, Hungary
feri@dtp.atomki.hu
[2] Institute for Computational Physics, University of Stuttgart, Pfaffenwaldring 27, 70569 Stuttgart, Germany
[3] Department of Fundamental Physics, University of Barcelona, Franques 1, 08028 Barcelona, Spain

The fibre bundle model is one of the most important theoretical approaches to investigate the fracture and breakdown of disordered media extensively used both by the engineering and physics community. We present the basic construction of the model and provide a brief overview of recent results focusing mainly on the physics literature. We discuss the limitations of the model to describe the failure of composite materials and present recent extensions of the model which overcome these problems making the model more realistic: we gradually enhance the fibre bundle model by generalizing the failure law, constitutive behavior, deformation state and way of interaction of fibres. We show that beyond the understanding of the fracture of fibre reinforced composites, these extensions of the fibre bundle model also address interesting problems for the statistical physics of fracture.

1 Introduction

The damage and fracture of disordered materials is a very important scientific and technological problem which has attracted an intensive research over the past decades. One of the first theoretical approaches to the problem was the fibre bundle model introduced by Peires in 1927 to understand the strength of cotton yarns [46]. In his pioneering work, Daniels provided the sound probabilistic formulation of the model and carried out a comprehensive study of bundles of threads assuming equal load sharing after subsequent failures [12]. In order to capture fatigue and creep effects, Coleman proposed a time dependent formulation of the model [7], assuming that the strength of loaded fibres is a decreasing function of time. Later on these early works initiated an intense research in both the engineering [47] and physics [6, 23] communities making fibre bundle models one of the most important theoretical approaches to the damage and fracture of disordered materials.

F. Kun et al.: *Extensions of Fibre Bundle Models*, Lect. Notes Phys. **705**, 57–92 (2007)
DOI 10.1007/3-540-35375-5_3

The development of fibre bundle models encountered two kinds of challenges: on the one hand it is important to work out realistic models of materials failure, which have a detailed representation of the microstructure of the material, the local stress fields and their complicated introduction. Such models make possible to clarify the effect of microscopic material parameters on the macroscopic response of solids. In this context, fibre bundle models served as a starting point to develop more realistic micromechanical models of the failure of fibre reinforced composites widely used by the modern aerospace and automobile industry. Analytical methods and numerical techniques have been developed making possible realistic treatment of even large scale fibrous structures. On the other hand, the damage and fracture of disordered materials addresses several interesting problems also for statistical physics. Embedding the failure and breakdown of materials into the general framework of statistical physics and clarifying its analogy to phase transitions and critical phenomena still keep scientists fascinated. Here fibre bundle models provide an excellent testing ground of ideas offering also the possibility of analytic solutions.

Fibre bundle models have been introduced to describe materials' degradation and failure, however, due to their simplicity, during the last two decades they also served as a general model of the breakdown of a broad class of disordered systems of many interacting elements subject to various types of external loads. Examples can be mentioned from magnets driven by an applied field [11, 71] through scale-free networks [10, 38] to earthquakes [63, 67] and social phenomena [11].

In this paper first we present the basic formulation of the classical fibre bundle model and briefly summarize the most important recent results obtained on the macroscopic response and microscopic damage process of disordered materials focusing on the physics literature. We discuss limitations of the model to describe the fracture of fibre reinforced composites and propose extensions which make the model more realistic. We gradually improve components of the model construction by generalizing the damage law, constitutive behavior, deformation state and interaction law of fibres. Finally, we give an overview of the applications of the extended fibre bundle model.

2 Fibre Bundle Model of Materials Failure

The construction of fibre bundle models (FBMs) is based on the following simplifying assumptions [2, 12, 28, 49, 53, 62]:

Discretization The disordered solid is represented as a discrete set of parallel fibres of number N organized on a regular lattice (square, triangular, ...), see Fig. 1. The fibres can solely support longitudinal deformation which allows to study only loading of the bundle parallel to fibres.

Failure Law When the bundle is subjected to an increasing external load, the fibres are assumed to have perfectly brittle response, i.e. they have linearly

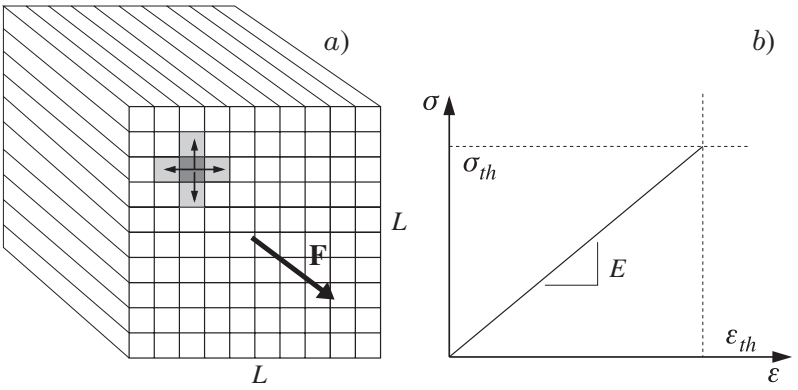

Fig. 1. (**a**) Set up of the classical fibre bundle model. Parallel fibres are assembled on a square lattice of size $L \times L$ loaded by an external force **F** parallel to the fibre direction. In the limiting case of very localized load sharing the load of a failed fibre (*dark grey*) is equally redistributed over its nearest intact neighbors (*light grey*). (**b**) Single fibres have linearly elastic behavior up to the failure load σ_{th}

elastic behavior until they break at a failure load $\sigma_{th}^i,\ i = 1, \ldots, N$ as it is illustrated in Fig. 2a. The elastic behavior of fibres is characterized by the Young modulus E, which is identical for all fibres. The failure of fibres is instantaneous and irreversible such that the load on broken fibres drops down to zero immediately at the instant of failure (see Fig. 2a), furthermore, broken fibres are never restored (no healing).

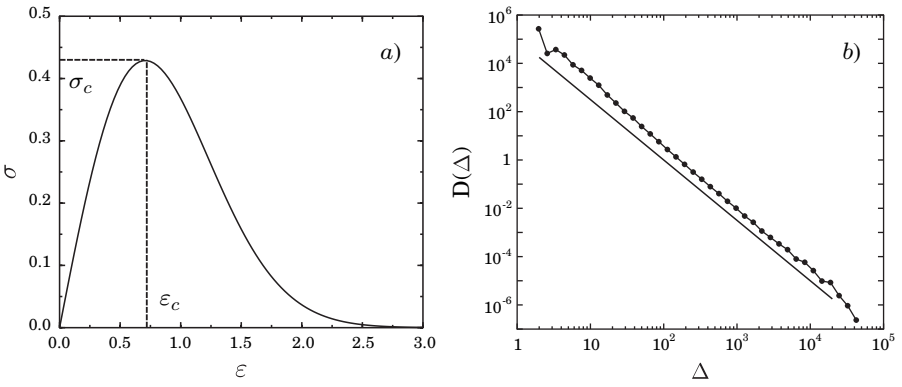

Fig. 2. (**a**) Macroscopic constitutive behavior of a fibre bundle with global load sharing (3) using Weibull distributed strength values σ_{th} ($m = 2$ and $\lambda = 1$). (**b**) Distribution D of burst sizes Δ obtained by computer simulations of a bundle of 10^7 fibres. A *straight line* of slope 2.5 is drawn to guide the eye

Load Sharing Rule After a fibre fails its load has to be shared by the remaining intact fibres. The range and form of interaction of fibres, also called load sharing rule, is a crucial component of the model which has a substantial effect on the micro and macro behavior of the bundle. Most of the studies in the literature are restricted to two extreme forms of the load sharing rule: (*i*) in the case of global load sharing (GLS), also called equal load sharing (ELS), the load is equally redistributed over all intact fibres in the bundle irrespective of their distance from the failed one. The GLS rule corresponds to the mean field approximation of FBM where the topology of the fibre bundle (like the square lattice structure in Fig. 2a) becomes irrelevant. Such a loading condition naturally arises when parallel fibres are loaded between perfectly rigid platens, like for the wire cable of an elevator. FBM with global load sharing is a usual starting point for more complex investigations since it makes possible to obtain the most important characteristic quantities of the bundle in closed analytic forms [22, 28, 53, 54, 62]. (*ii*) In the other extreme of the local load sharing (LLS), the entire load of the failed fibre is redistributed equally over its local neighborhood (usually nearest neighbors) in the lattice considered, leading to stress concentrations along failed regions (see Fig. 1a). Due to the non-trivial spatial correlations, the analytic treatment of LLS bundles has serious limitations [17, 20, 49], most of the studies here rely on large scale computer simulations [9, 18, 21, 26]. Such localized load sharing occurs when a bundle of fibres is loaded between plates of finite compliance [4, 13, 19].

Distribution of Failure Thresholds The strength of fibres σ_{th}^{i}, i.e. the value of the local load at which they break, is an independent identically distributed random variable with the probability density $p(\sigma_{th})$ and distribution function $P(\sigma_{th}) = \int_{\sigma_{th}^{min}}^{\sigma_{th}^{\max}} p(x)dx$. The randomness of breaking thresholds is assumed to represent the disorder of heterogeneous materials, and hence, it is practically the only component of the classical FBM where material dependent features (e.g. amount of disorder) can be taken into account. For the disordered breaking thresholds the uniform distribution between 0 and 1 with the density and distribution functions

$$p(\sigma_{th}) = 1, \qquad P(\sigma_{th}) = \sigma_{th} \ , \tag{1}$$

is a usual starting point in most of the investigations. Another widely used distribution in FBMs is the Weibull distribution

$$P(\sigma_{th}) = 1 - \exp\left[-\left(\frac{\sigma_{th}}{\lambda}\right)^{m}\right] , \tag{2}$$

where m and λ denote the Weibull index and scale parameter, respectively. Besides its physical ground [6, 23], the Weibull distribution has the advantage from the viewpoint of modelling that the amount of disorder can be controlled by varying the Weibull index m.

Time Dependence According to the time dependence of the fibre strength, two classes of FBMs can be distinguished: in static fibre bundles the breaking thresholds are constant during the entire loading history of the bundle. In order to model a certain type of creep rupture and fatigue behavior of materials, time dependent strength of fibres has been introduced [7, 34, 35, 42, 65].

In spite of their simplicity, FBMs provided a deeper understanding of the breakdown of heterogeneous materials revealing important basic features of the failure process. In the following we briefly summarize the most important results of FBMs on the microscopic failure process and macroscopic response of disordered materials under quasistatic loading conditions. Loading of a parallel bundle of fibres can be performed in two substantially different ways: when the deformation ε of the bundle is controlled externally, the load on single fibres σ_i is always determined by the externally imposed deformation ε as $\sigma_i = E\varepsilon$, i.e. no load sharing occurs and consequently the fibres break one-by-one in the increasing order of their breaking thresholds. At a given deformation ε the fibres with breaking thresholds $\sigma_{th}^i < E\varepsilon$ are broken, furthermore, all intact fibres keep the equal load $E\varepsilon$. Hence, the macroscopic constitutive behavior $\sigma(\varepsilon)$ of the FBMs can be cast in the form

$$\sigma(\varepsilon) = E\varepsilon\left[1 - P(E\varepsilon)\right] \ , \tag{3}$$

where $[1 - P(E\varepsilon)]$ is the fraction of intact fibres at the deformation ε [11, 62]. A representative example of $\sigma(\varepsilon)$ is presented in Fig. 2a for the case of Weibull distributed strength values with $m = 2$ and $\lambda = 1$. Under stress controlled conditions when the load is gradually increased externally, a more complex damage process occurs starting with the breaking of the weakest fibre. After each fibre breaking the load dropped by the broken fibre has to be redistributed over the surviving intact ones. Assuming global load sharing (equal load sharing), all intact fibresndexfibre bundle model receive the same load increment which might cause secondary fibre breakings. The subsequent load redistribution after consecutive fibre failures can lead to an entire avalanche of breakings which can stop after a certain number of fibres keeping the integrity of the bundle, or can be catastrophic resulting in the macroscopic failure of the entire system. Hence, under stress controlled loading, the constitutive curve (3) can only be realized up to the maximum, where a catastrophic avalanche occurs breaking all the remaining fibres [22, 24, 28, 54]. It has been shown analytically that for a broad class of disorder distributions P under GLS conditions the macroscopic constitutive curve $\sigma(\varepsilon)$ of FBMs has a quadratic maximum whose position and value define the critical strain ε_c and stress σ_c of the bundle [11, 62], respectively (see Fig. 2a). Increasing the size N of finite bundles, the global strength $\sigma_c(N)$ rapidly converges to the finite non-zero strength of the infinite bundle [12, 49, 62].

When the load sharing is localized the macroscopic response of the bundle becomes more brittle, i.e. the constitutive curve $\sigma(\varepsilon)$ of the LLS bundle follows its GLS counterpart but the macroscopic failure occurs at a lower critical stress $\sigma_c^{LLS} < \sigma_c^{GLS}$, which is preceded by only a weak non-linearity [26]. Large scale

computer simulations revealed that in the thermodynamic limit $N \to \infty$, the strength of LLS bundles tends to zero as $1/(\ln N)$.

On the micro-level the spatial and temporal evolution of damage shows also a strong dependence on the range of load redistribution: when the excess load of failed fibres is redistributed globally (GLS) no spatial correlations arise, i.e. fibre breaking proceeds in a completely stochastic manner in space which results in randomly nucleated clusters of broken fibres analogous to percolation. Under stress controlled loading conditions, the subsequent load redistribution results in a bursting activity preceding the macroscopic failure of the bundle. For equal load sharing it has been proven analytically that the distribution $D(\Delta)$ of burst sizes Δ recorded during the entire course of loading has a universal power law behavior

$$D(\Delta) \sim \Delta^{-\alpha} , \tag{4}$$

with an exponent $\alpha = 5/2$ independent of the disorder distribution P [22, 28, 51], see Fig. 2b. The power law distribution of bursts prevails also for more complicated long range interactions (like in the fuse model [3, 45]) but localized load sharing results in a rapid decrease of $D(\Delta)$ and in a dependence on the specific form of disorder P [18].

In recent years several novel aspects of breakdown phenomena have been revealed in the framework of FBMs: It has been shown that thermal noise leads to the reduction of the strength of materials, furthermore, thermally activated cracking gives rise to sub-critical crack growth and a finite lifetime of materials [59, 61]. When avalanches of fibre failures are solely recorded in the vicinity of the point of macroscopic failure, i.e. the strength distribution of the remaining intact fibres is close to critical, the avalanche size distribution $D(\Delta)$ proved to show a crossover from the power law of exponent 5/2 to another power law regime with a lower exponent 3/2 [55, 56]. The connectivity properties of the bundle turned out to play an important role in breakdown processes, i.e. determining the local interacting partners of fibres in a bundle by a Barabasi-Albert network instead of a regular lattice, the failure process is substantially different [10].

FBMs played also a crucial role to clarify the fundamental problem of the relation of breakdown of disordered materials to critical phenomena [2, 5, 37, 68, 69, 71] and self organized criticality [36]. When fibre bundles with global load sharing approach the point of macroscopic failure under a quasistatically increasing load, it was found that microscopic quantities of the bundle such as the distribution of bursts of fibre breakings show a scaling behavior typical for continuous phase transitions [5, 19, 22, 28, 37, 51, 52, 53]. Since at the same time macroscopic quantities like the Young modulus of the bundle proved to have a finite jump, it was suggested that the macroscopic failure of GLS systems occurs analogous to first order phase transitions close to a spinodal [33, 69, 70, 71]. An interesting mapping of the fracture process of fibre bundles to Ising-like models widely studied in statistical physics has been suggested

[53, 57, 66], which provides further hints to embed fracture phenomena into the general framework of statistical physics.

2.1 Why Extensions are Necessary?

A very important type of materials for which fibre bundle models are of outstanding importance are the so-called fibre reinforced composites (FRC) which have two ingredients, i.e. a matrix or carrier material in which thin fibres of another material are embedded in a certain geometrical arrangement. The modern automotive and aerospace industries use a large amount of fibre reinforced composites due to their very good mass specific properties, i.e. FRCs provide a very high strength at a relatively low mass and they sustain these properties also under extreme conditions (high temperature, pressure). The mechanical performance of FRC can be well controlled by the properties of the fibre and matrix materials, and by the fabrication of the fibre-matrix interface and the geometrical structure of the composite. This flexibility makes possible the design and tailoring of special purpose structural materials that best fit to the demands of applications. Fig. 3*a*) presents the structure of the carbon fibre reinforced silicon carbide composite (C/C-SiC) extensively used by the aerospace industry. It can be observed that parallel bundles of long carbon fibres (diameter $\sim 10\,\mu$m) are embedded in the silicon-carbide ceramic matrix [30]. Reinforcement by fibrous structures can also be found in nature in various types of plants. The structure of soft-wood of the species spruce is shown in Fig. 3*b*) as a representative example [15]. Theoretical studies of the fracture of composites encounter various challenges: on the one hand, applications of materials in construction components require the development of

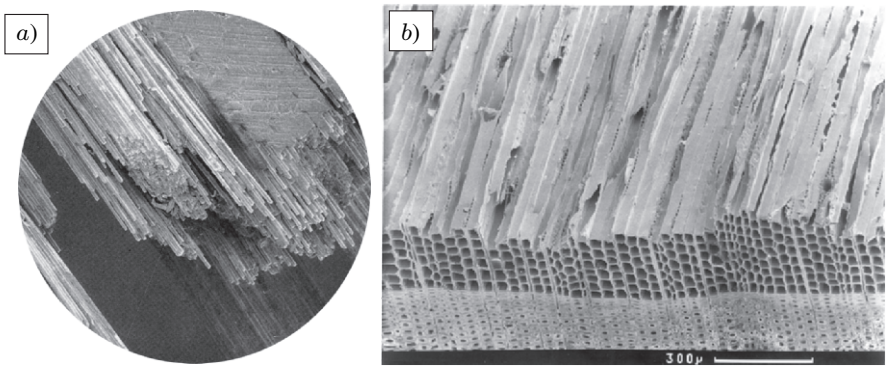

Fig. 3. (**a**) Structure of a fibre reinforced composite (Carbon fibre reinforced silicon-carbide). Long parallel fibres are embedded in a matrix material [30]. (**b**) The soft-wood is an example of natural fibrous materials. The fibres are tubes whose wall gets thicker as the tree grows [15]

analytical and numerical models which are able to predict the damage histories of loaded specimens in terms of the characteristic microscopic parameters of the constituents. On the other hand, it is important to reveal universal aspects of the fracture of composites, which are independent of specific material properties relevant on the microlevel. Such universal quantities can help to extract the relevant information from measured data and make possible to design monitoring techniques of the gradual degradation of composites' strength and construct methods of forecasting catastrophic failure events.

When fibre composites are subject to an external load parallel to the fibre direction, most of the load is carried by the fibres, the matrix material and properties of the fibre-matrix interface mainly determine the interaction (load transfer) among fibres, which make FBMs the most adequate approach to describe the fracture process of FRCs [8, 30, 48, 50]. As it has been presented above, in their basic setup FBMs provide a rather idealized representation of the behavior of disordered brittle materials. In order to obtain a more realistic description especially for the failure of composites, FBMs have to be enhanced by capturing a more detailed picture of the mechanical behavior of the constituents, the evolution of the local stress field and its interaction with the disordered material properties. In the following we outline important aspects of the mechanical performance of FRCs which cannot be described in the framework of the classical FBM but call for extensions of the model.

In applications, long fibre composites loaded parallel to the direction of fibres are often found to undergo a gradual degradation process such that the macroscopic constitutive curve $\sigma(\varepsilon)$ of the composite develops a plateau regime and the global failure is preceded by strain hardening. This effect becomes especially important when the fibre bundle has a hierarchical organization and the failure mechanisms relevant at the lower length scales (at the scale of fibres) gradually activate the breaking of higher order substructures (sub-bundles, bundles, and plies) of the system. When fibres are embedded in a matrix material, after a fibre breaks, the fibre-matrix interface debonds in the vicinity of the crack [49]. Due to the frictional contact at the interface, the load of failed fibres builds up again over a certain stress recovery length so that the broken fibre can still contribute to the overall load bearing capacity of the system.

Under high steady stresses, materials may undergo time dependent deformation resulting in failure called creep rupture, which determines the long time performance and limits the lifetime of construction elements. This complex time dependent macroscopic behavior emerges as the result of the interplay of the time dependent deformation of the constituents and the gradual accumulation of damage.

In applications solid blocks are often joined together by welding or glueing of the interfaces which are expected to sustain various types of external loads. Interfacial failure also occurs in fibre reinforced composites, where debonding of the fibre-matrix interface can even be the dominating damage mechanism when the composite is sheared. When interfaces of solids are subject to

shear the interface elements suffer not only longitudinal deformation (compression and elongation) but also bending deformation. Such complex deformation states cannot be captured by discretizing the interface in terms of fibres which can only support longitudinal deformation.

As it has been discussed in Sect. 2, the range and functional form of load redistribution of fibres play a crucial role in the failure process of the model. A realistic description of load transfer following fibre failure should obviously fall somewhere between the limiting cases of the widely studied global and local load redistributions. The importance of the accurate description of the load transfer from broken to intact fibres has already been recognized by Daniels for cotton yarns [12].

In the following we present extensions of the classical fibre bundle model gradually improving components of the model construction outlined in Sect. 2: (*I*) In order to understand the damage mechanism that lead to plateau formation and strain hardening of the macroscopic response of quasi-brittle materials, we modify the failure law of fibres in FBMs assuming that individual fibres undergo a gradual degradation process reducing their Young modulus in a multiplicative way in consecutive failure events. (*II*) To describe the damage enhanced creep of fibrous materials we introduce time dependent deformation behavior for the fibres and combine it with strain controlled breaking in a global load sharing framework. (*III*) We show that more complex deformation states (besides the longitudinal deformation) and failure processes can be described by FBMs when fibres are substituted by beams, which can be stretched, compressed and bent at the two ends. We apply the bundle of beams to investigate the fracture of glued interfaces of solid blocks. (*IV*) Motivated by the results of fracture mechanics on the stress distribution around cracks, we introduce a one-parameter load transfer function for fibres, which can interpolate between the limiting cases of global and local load sharing. The value of the parameter of the load transfer function controls the effective range of interaction of broken and intact fibres. We apply the variable range of load sharing approach also to clarify universal aspects of the creep rupture of composites. Figure 4 gives an overview of the structure of the remaining part of the paper. We note that since in the framework of the classical fibre bundle model no effect of the matrix material between fibres is taken into account, the model is also called dry fibre bundle model (DFBM) in the literature in order to distinguish it from the improved variants.

3 Gradual Degradation of Fibre Strength

In the following we introduce a so-called continuous damage fibre bundle model as an extension of the classical FBM by generalizing the damage law of fibres. We assume that the stiffness of fibres gradually decreases in consecutive failure events. We show that varying its parameters, the model provides a broad spectrum of macroscopic constitutive behaviors from plasticity to

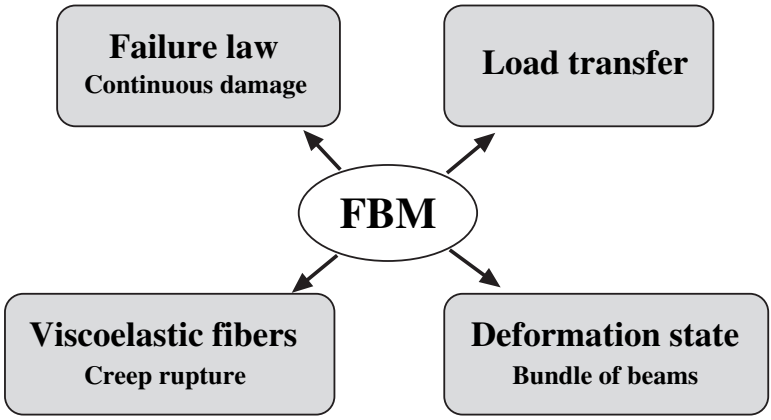

Fig. 4. Extensions of fibre bundle models: we gradually enhance FBMs by generalizing the damage law, the load transfer, the constitutive behavior and deformation state of the fibres

strain hardening in qualitative agreement with experiments. To reveal the microscopic process of damage we construct a simulation techniques and obtain the statistics of bursts of fibre breakings. We find that burst distributions show a power law behavior but surprisingly the exponent can be different from the well know mean field exponent of FBMs [24, 33].

3.1 Continuous Damage Fibre Bundle Model

Based on the classical fibre bundle model, the continuous damage model is composed of N parallel fibres with identical Young-modulus E and random failure thresholds σ_{th}^i, $i = 1, \ldots, N$ of probability density p and distribution function P (see also Fig. 1 for illustration). The fibres are assumed to have linear elastic behavior up to breaking (brittle failure). Under uniaxial loading of the specimen a fibre fails if it experiences a load larger than its breaking threshold σ_{th}^i. We generalize the failure law of DFBM by assuming that at the failure point the stiffness of the fibre gets reduced by a factor a, where $0 \leq a < 1$, i.e. the stiffness of the fibre after failure is aE. In principle, a fibre can now fail more than once and the maximum number $k_{\max}$ of failures allowed for fibres is a parameter of the model. Once a fibre has failed, its damage threshold σ_{th}^i can either be kept constant for the further breakings (quenched disorder) or new failure thresholds of the same distribution can be chosen (annealed disorder), which can model some microscopic rearrangement of the material after failure. The damage law of the model is illustrated in Fig. 5 for both types of disorder, which should be compared to Fig. 1. The characterization of damage by a continuous parameter corresponds to describe the system on length scales larger than the typical crack size. This can be interpreted such

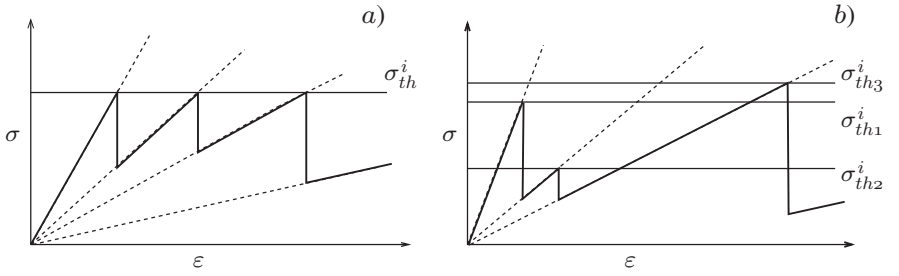

Fig. 5. The damage law of a single fibre of the continuous damage model when multiple failure is allowed (**a**) for quenched, and (**b**) for annealed disorder. The *horizontal lines* indicate the damage threshold σ_{th}^i. See also [24, 33]

that the smallest elements of the model are fibres and the continuous damage is due to cracking inside fibres. However, the model can also be considered as the discretization of the system on length scales larger than the size of single fibres, so that one element of the model consists of a collection of fibres with matrix material in between. In this case the microscopic damage mechanism resulting in multiple failure of the elements is the gradual cracking of matrix and the breaking of fibres. In the following we refer to the elements of the continuous damage FBM as fibres, but we have the above two possible interpretations in mind. After failure the fibre skips a certain amount of load which has to be taken by the other fibres. For the load redistribution we assume infinite range of interaction among fibres (mean field approach), furthermore, equal strain condition is imposed which implies that stiffer fibres of the system carry more load. At a strain ε, the load of fibre i that has failed $k(i)$ times reads as

$$f_i(\varepsilon) = Ea^{k(i)}\varepsilon \,, \tag{5}$$

where $Ea^{k(i)}$ is the actual stiffness of fibre i. It is important to note that, in spite of the infinite interaction range, (5) is different from the usual global load sharing (GLS) where all the intact fibres carry always the same amount of load (see Sect. 2). In the following the initial fibre stiffness E will be set to unity.

3.2 Macroscopic Constitutive Behavior

The key quantity to determine the macroscopic constitutive behavior of the continuous damage fibre bundle model (CDFBM) and to characterize its microscopic damage process, is the probability $P_k(\varepsilon)$ that during the loading of a specimen an arbitrarily chosen fibre failed precisely k-times at a strain ε. Here $k = 0, \ldots, k_{\max}$ denotes the failure index, and $k = 0$ is assigned to the intact fibres. $P_k(\varepsilon)$ can be cast in the following form for *annealed disorder*

$$P_k(\varepsilon) = \left[1 - P(a^k\varepsilon)\right] \prod_{j=0}^{k-1} P(a^j\varepsilon) \ , \qquad (6)$$
$$\text{for} \qquad 0 \le k \le k_{\max} - 1 \ ,$$
$$\text{and} \qquad P_{k_{\max}}(\varepsilon) = \prod_{j=0}^{k_{\max}-1} P(a^j\varepsilon) \ ,$$

and for *quenched disorder*

$$P_0(\varepsilon) = 1 - P(\varepsilon) \ ,$$
$$P_k(\varepsilon) = P(a^{k-1}\varepsilon) - P(a^k\varepsilon) \ , \text{ for } 1 \le k \le k_{\max} - 1 \ , \qquad (7)$$
$$\text{and} \quad P_{k_{\max}}(\varepsilon) = P(a^{k_{\max}-1}\varepsilon) \ .$$

It can easily be seen that the probabilities (6,7) fulfill the normalization condition $\sum_{k=0}^{k_{\max}} P_k(\varepsilon) = 1$. Average quantities of the fibre ensemble during a loading process can be calculated using the probabilities (6,7). For instance, the average load on a fibre F/N at a given strain ε reads as

$$\frac{F}{N} = \varepsilon \left[\sum_{k=0}^{k_{\max}} a^k P_k(\varepsilon) \right] \ , \qquad (8)$$

which provides the macroscopic constitutive behavior of the model. The single terms in the sum give the load carried by the subset of fibres of failure index k. The variants of fibre bundle models used widespread in the literature can be recovered by special choices of the parameters $k_{\max}$ and a of the model. A micromechanical model of composites [8, 30, 48, 50] can be obtained with the parameter values $k_{\max} = 1$, $a \neq 0$

$$\frac{F}{N} = \varepsilon \left[1 - P(\varepsilon)\right] + a\varepsilon P(\varepsilon) \ , \qquad (9)$$

while setting $k_{\max} = 1$, $a = 0$, i.e. skipping the second term in (9) results in the classical dry bundle model of Daniels [12] with the constitutive behavior (3). In Fig. 6 we show the explicit form of the constitutive law with annealed disorder for different values of $k_{\max}$ in the case of the Weibull distribution (2). The parameter values are set to $m = 2$, $\lambda = 1$ in all the calculations.

Note that in the constitutive equation (8) the term of the highest failure index $k_{\max}$ can be conceived such that the fibres have a residual stiffness of $a^{k_{\max}}$ after having failed $k_{\max}$ times. This residual stiffness results in a hardening of the material, hence, the F/N curves in Fig. 6a asymptotically tend to straight lines with a slope $a^{k_{\max}}$. Increasing $k_{\max}$ the hardening part of the constitutive behavior is preceded by a longer and longer plastic plateau, and in the limiting case of $k_{\max} \to \infty$ the materials behavior becomes completely plasticity. A similar plateau and asymptotic linear hardening has been observed in brittle matrix composites, where the multiple cracking of matrix

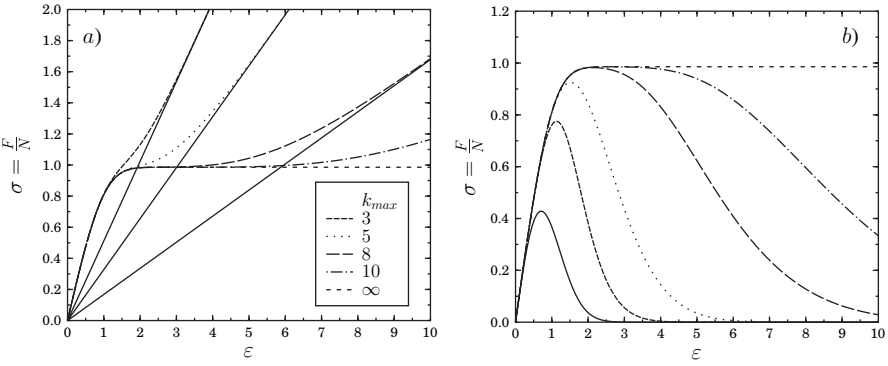

Fig. 6. Constitutive behavior of the model of annealed disorder (**a**) with (**b**) without residual stiffness at $a = 0.8$ for different values of $k_{\max}$. In (**b**) the lowest curve presents the constitutive behavior of the classical dry bundle model for comparison

turned out to be responsible for the relatively broad plateau of the constitutive behavior, and the asymptotic linear part is due to the linear elastic behavior of fibres remaining intact after matrix cracking [16].

In order to describe macroscopic cracking and global failure of a specimen instead of hardening, the residual stiffness of the fibres has to be set to zero after a maximum number k^* of allowed failures [33, 72]. In this case the constitutive law can be obtained from the general form (8) by replacing $k_{\max}$ in the upper limit of the sum by $k^* - 1$. A comparison of the constitutive laws of the dry and continuous damage FBM with global failure is presented in Fig. 6b. One can observe that the dry FBM constitutive law has a relatively sharp maximum, while the continuous damage FBM curves exhibit a plateau whose length increases with increasing k^*. Note that the maximum value of F/N corresponds to the macroscopic strength of the material, furthermore, in stress controlled experiments the plateau and the decreasing part of the curves cannot be reached. However, in strain controlled experiments the plateau and the decreasing regime can also be realized. The value of the driving stress $\sigma \equiv F/N$ corresponding to the plastic plateau, and the length of the plateau are determined by the damage parameter a, and by $k_{\max}$, k^*: Decreasing a at a fixed $k_{\max}, k^*$, or increasing $k_{\max}, k^*$ at a fixed a increase the plateau's length.

3.3 Simulation Techniques

Due to the difficulties of the analytic treatment, we develop a simulation technique and explore numerically the properties of bursts of fibre breakings in our continuous damage fibre bundle model. The interaction of fibres, i.e. the way of load redistribution is crucial for the avalanche activity. A very important property of CDFBM is that in spite of the infinite range of interaction

the load on intact fibres is not equal, but stiffer fibres carry more load, furthermore, for quenched disorder damage localization occurs, which can affect also the avalanche activity [24, 33].

To implement the quasi-static loading of a specimen of N fibres in the framework of CDFBM, the local load on the fibres f_i has to be expressed in terms of the external driving F. Making use of (5) it follows that

$$F = \sum_{i=1}^{N} f_i = \varepsilon \sum_{i=1}^{N} a^{k(i)} \ , \tag{10}$$

and hence, the strain and the local load on fibres can be obtained as

$$\varepsilon = \frac{F}{\sum_{i=1}^{N} a^{k(i)}}, \quad f_i = F \frac{a^{k(i)}}{\sum_{i=1}^{N} a^{k(i)}} \ , \tag{11}$$

when the external load F is controlled. The simulation of the quasi-static loading proceeds as follows: in a given stable state of the system we determine the load on the fibres f_i from the external load F using (11). The next fibre to break can be found as

$$r = \frac{\sigma_{th}^{i^*}}{f_{i^*}} = \min_i \frac{\sigma_{th}^{i}}{f_i}, \qquad r > 1 \ , \tag{12}$$

i.e. that fibre breaks for which the ratio σ_{th}^{i}/f_i is the smallest. Here i^* denotes the index of the fibre to break, σ_{th}^{i} is the damage threshold of fibre i, and f_i is the local load on it. To ensure that the local load of a fibre is proportional to its stiffness, the external load has to be increased in a multiplicative way, so that $F \to rF$ is imposed, and the failure index of fibre i^* is increased by one $k(i^*) \to k(i^*) + 1$. After the breaking of fibre i^*, the load f_i carried by the fibres has to be recalculated making use of (11), which provides also the correct load redistribution of the model. If there are fibres in the state obtained, whose load exceeds the local breaking threshold, they fail, i.e. their failure index is increased by 1 and the local load is again recalculated until a stable state is obtained. A fibre cannot break any longer if its failure index k has reached k^* or $k_{\max}$ during the course of the simulations. This dynamics gives rise to a complex avalanche activity of fibre breaks, which is also affected by the type of disorder. The size of an avalanche Δ is defined as the number of breakings initiated by a single failure due to an external load increment.

3.4 Bursts of Fibres Breakings

Computer simulations revealed that varying the two parameters of the model $k_{\max}, a$, or k^*, a and the type of disorder, the CDFBM shows an interesting variety of avalanche activities, characterized by different shapes of the avalanche

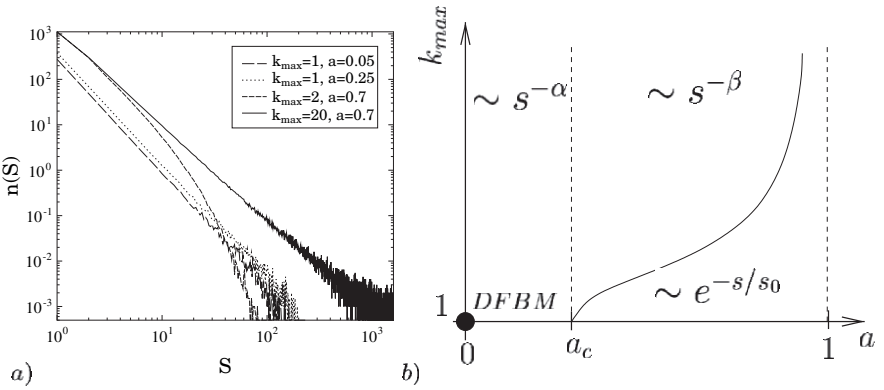

Fig. 7. (**a**) Avalanche size distributions for different values of $k_{\max}$ and a when fibres have remaining stiffness and the disorder is annealed. The number of fibres was $N = 1600$ and averages were made over 2000 samples. The number of avalanches D of size Δ are shown to demonstrate also how the total number of avalanches changes. (**b**) Phase diagram for the continuous damage model with remaining stiffness for both types of disorder. The functional form of the avalanche statistics is given in the parameter regimes. The location of DFBM in the parameter space is also indicated

size distributions. In Fig. 7a the histograms $D(\Delta)$ of the avalanche sizes Δ are shown which were obtained for a system of remaining stiffness and annealed disorder with Weibull parameters $m = 2$, $\lambda = 1$. Since in the limiting case of $a \to 0$ the CDFBM recovers the global load sharing dry fibre bundle model, in Fig. 7a the curves with small a and $k_{\max} = 1$ are power laws with an exponent $\alpha = 5/2$ in agreement with the analytic results [22, 28, 54]. Increasing the value of a at a fixed $k_{\max}$ only gives rise to a larger number of avalanches, i.e. parallel straight lines are obtained on a double logarithmic plot, but the functional form of $D(\Delta)$ does not change. However, when a exceeds a critical value a_c ($a_c \approx 0.3$ was obtained with the Weibull parameters specified above), the avalanche statistics drastically changes. At a fixed $a > a_c$ when $k_{\max}$ is smaller than a specific value $k_c(a)$, the avalanche sizes show exponential distribution, while above $k_c(a)$ the distribution takes a power law form with an exponent $\beta = 2.12 \pm 0.05$. Based on the above results of simulations a phase diagram is constructed which summarizes the properties of avalanches with respect to the parameters of the model. Figure 7 demonstrates the existence of three different regimes. If the damage parameter a is smaller than a_c, the dynamics of avalanches is close to the simple DFBM characterized by a power law of the mean field exponent $\alpha = 5/2$. However, for $a > a_c$ the avalanche size distribution depends on the number of failures $k_{\max}$ allowed. The curve of $k_c(a)$ in the phase diagram separates two different regimes. For the parameter regime below the curve, avalanche distributions with an exponential shape were obtained. However, the parameter regime above $k_c(a)$

is characterized by a power law distribution of avalanches with a constant exponent $\beta = 2.12 \pm 0.05$ significantly different from the mean field exponent $\alpha = 5/2$ [22, 28, 54]. It is important to emphasize that the overall shape of the phase diagram is independent of the type of the disorder (annealed or quenched), moreover, the specific values $a_c \approx 0.3$ and $k_c(a)$ depend on the details of the disorder distribution $p(\sigma_{th})$.

4 Variable Range of Load Sharing

In this section we introduce a one-parameter load transfer function to obtain a more realistic description of the interaction of fibres. Varying its parameter, the load transfer function interpolates between the two limiting cases of load redistribution, i.e. the global and the local load sharing schemes widely studied in the literature. We show that varying the effective range of interaction a crossover occurs from mean field to short range behavior. To explore the properties of the two regimes and the emergence of the crossover in between, a comprehensive numerical study of the model is performed. We study the dependence of the ultimate strength of the material on the system size and found that the system has only one nonzero critical point in the thermodynamic limit. When no critical point exits, the ultimate strength of the material goes to zero exactly as in local load sharing models as $\sim 1 \ln(N)$, with increasing system size N. We also study the distribution of avalanches and cluster sizes for the two distinct regimes and perform a moments analysis to accurately obtain the crossover value [26].

4.1 Load Transfer Function

The fracture of heterogeneous systems is characterized by the highly localized concentration of stresses at the crack tips that makes possible the nucleation of new micro-cracks at these regions leading to the growth of the crack and final failure of the system. In elastic materials, the stress distribution around cracks follows a power law

$$\sigma_{add} \sim r^{-\gamma} \,, \tag{13}$$

where σ_{add} is the stress increase on a material element at a distance r from the crack tip. Motivated by the above result of fracture mechanics we extend the fibre bundle model introducing a load sharing rule of the form of (13).

In the model we suppose that, in general, all intact fibres have a nonzero probability of being affected by the ongoing failure event, and that the additional load received by an intact fibre i depends on its distance r_{ij} from fibre j which has just been broken. Furthermore, elastic interaction is assumed between fibres such that the load received by a fibre follows the power law form.

Hence, in our discrete model the stress-transfer function $F(r_{ij}, \gamma)$ takes the form

$$F(r_{ij}, \gamma) = Z r_{ij}^{-\gamma} , \tag{14}$$

where γ is an adjustable parameter and r_{ij} is the distance of fibre i to the rupture point (x_j, y_j), i.e., $r_{ij} = \sqrt{(x_i - x_j)^2 + (y_i - y_j)^2}$ in 2D. Z is given by the normalization condition $Z = (\sum_{i \in I} r_{ij}^{-\gamma})^{-1}$, where the sum runs over the set I of all intact elements. For simplicity, periodic boundary conditions with the minimum image convention are used (no Ewald summation is performed [1]) so that the largest r value is $R_{\max} = \frac{\sqrt{2}(L-1)}{2}$, where L is the linear size of the system. It is easy to see that in the limits $\gamma \to 0$ and $\gamma \to \infty$ the load transfer function (14) recovers the two extreme cases of load redistribution of fibre bundle models, i.e. the global and the local load sharing, respectively. We should note here that, strictly speaking, for all γ different from the two limits above, the range of interaction covers the whole lattice. However, when changing the exponent, one moves from a very localized *effective* interaction to a truly global one as γ approaches zero. So, we will refer henceforth to a change in the *effective* range of interaction.

4.2 Macroscopic Strength of Bundles

We have carried out large scale computer simulations of the model described above in two dimensions. The fibres with Weibull distributed strength values (2) are organized on a square lattice of linear size L using periodic boundary conditions (see also Fig. 1). Computer simulations were performed varying the effective range of interaction γ over a broad interval recording the avalanche size distribution, the cluster size distribution and the ultimate strength of the bundle for several system sizes L. Each numerical simulation was repeated over at least 50 different realizations of the disorder distribution with the parameter values $m = 2$ and $\lambda = 1$ of the Weibull distribution.

Figure 8a shows the ultimate strength σ_c of the fibre bundle for different values of the parameter γ and several system sizes from $L = 33$ to $L = 257$. Clearly, two distinct regimes can be distinguished: For small γ, the strength σ_c is independent, within statistical errors, of both the effective range of interaction γ and the system size L. At a given point $\gamma = \gamma_c$ a crossover is observed, where γ_c falls in the vicinity of $\gamma = 2$. The region $\gamma > \gamma_c$ might eventually be further divided into two parts, the first region characterized by the dependence of the ultimate strength of the bundle on both the system size and the effective range of interaction; and a second region where σ_c only depends on the system size. This would mean that there might be two transition points in the model, for which the system displays qualitatively and quantitatively different behaviors. For $\gamma \leq \gamma_c$ the ultimate strength of the bundle behaves as in the limiting case of global load sharing, whereas for $\gamma \geq \gamma_c$ the local load sharing behavior seems to prevail. Nevertheless, the most important feature is that when decreasing the effective range of interaction in the thermodynamic

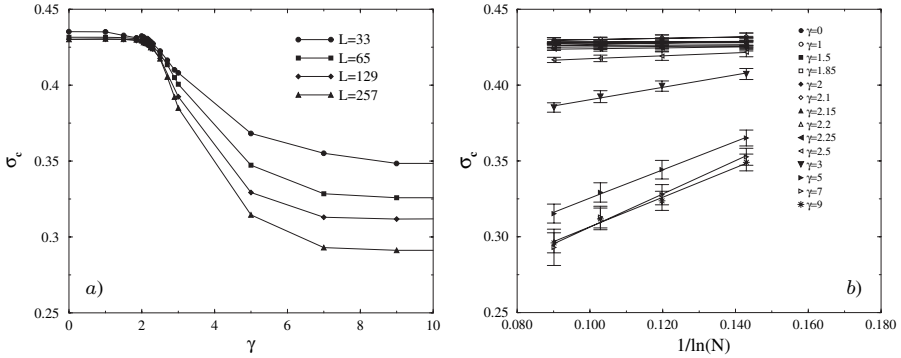

Fig. 8. (**a**) Macroscopic strength σ_c of fibre bundles of different size L as a function of the exponent γ of the load transfer function (14). (**b**) Variation of σ_c with the number of fibres of the bundle N at different γ values

limit, for $\gamma > \gamma_c$, the critical load is zero. This observation is further supported by Fig. 8(b), where we have plotted the evolution of σ_c as a function of $1/\ln N$ for different values of the exponent γ. Here, the two limiting cases are again clearly differentiated. For large γ all curves decreases when $N \to \infty$ as

$$\sigma_c(N) \sim \frac{\alpha}{\ln N} \ . \tag{15}$$

This qualifies for a genuine short range behavior as found in LLS models where the same relation was obtained for the asymptotic strength of the bundle [49]. It is worth noting that in the model we are analyzing, the limiting case of local load sharing corresponds to models in which short range interactions are considered to affect the nearest and the next-nearest neighbors only. In the transition region, the maximum load the system can support also decreases as we approach the thermodynamic limit, but in this case much slower than for $\gamma \gg \gamma_c$. It has been pointed out that for some modalities of stress transfer, which can be considered as intermediate between GLS and LLS, σ_c decreases for large system sizes following the relation $\sigma_c \sim 1/\ln(\ln N)$ as in the case of hierarchical load transfer models [41]. In our case, we have fitted our results with this relation but we have not obtained a single collapsed curve because the slopes continuously vary until the LLS limit is reached. Finally, the region where the ultimate stress does not depend on the system size shows the behavior expected for the standard GLS model, where the critical load can be exactly computed as $\sigma_c = (me)^{-1/m}$ for the Weibull distribution. The numerical values obtained for $m = 2$ are in good agreement with this later expression.

4.3 Microstructure of Damage

In order to characterize the fracture process under the quasistatically increasing external load we analyzed the cluster structure of broken fibres. The clusters formed during the evolution of the fracture process are sets of spatially connected broken sites on the square lattice [33, 70, 71]. We consider the clusters just before the global failure and they are defined taking into account solely nearest neighbor connections. As it has been discussed in Sect. 2, the case of global load sharing does not assume any spatial structure of fibres since it corresponds to the mean field approach. However, in our case it is obtained as a limiting case of a local load sharing model on a square lattice, which justifies the cluster analysis also for GLS. Figure 9 illustrates how the cluster structure just before complete breakdown changes for various values

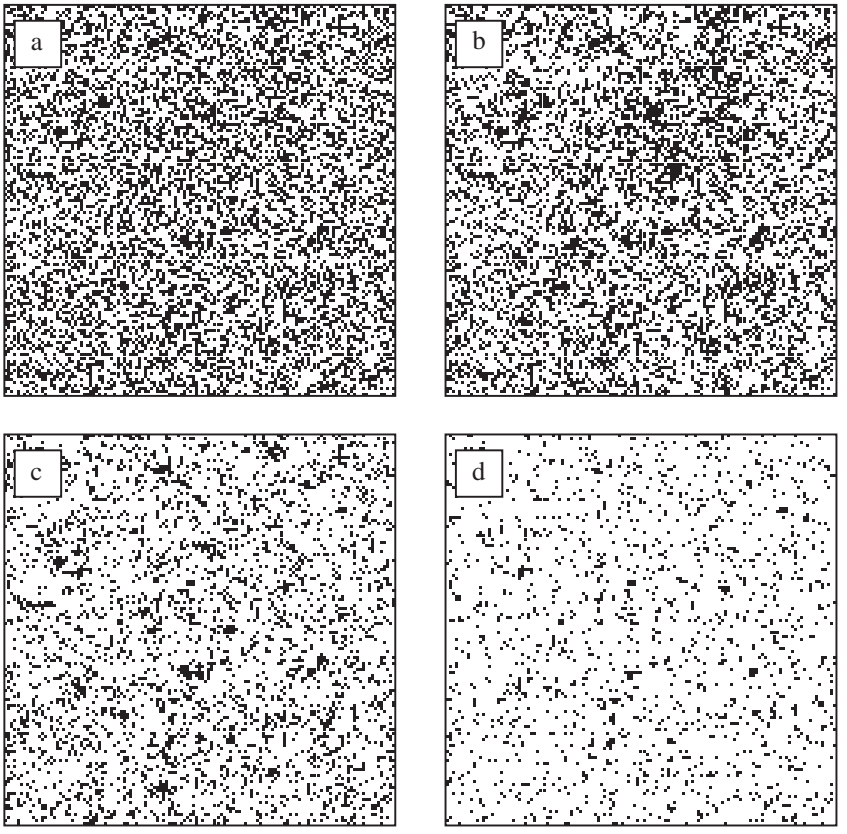

Fig. 9. Snapshots of the clusters of broken fibres (*black dots*) just before complete breakdown occurs. A clear change of the cluster structure can be observed. The values of γ are: (**a**) $\gamma = 0$, (**b**) $\gamma_c = 2.2$, (**c**) $\gamma = 3.0$, and (**d**) $\gamma = 9.0$

of γ. In the limit where the long range interaction dominates, the clusters are randomly distributed on the lattice indicating that there is no correlated crack growth in the system and no stress concentration occurs. The cluster structure of the limiting case of $\gamma = 0$ can be mapped to percolation clusters on a square lattice generated with the probability $0 < P(\sigma_c) < 1$, where σ_c is the fracture strength of the fibre bundle. However, the value of $P(\sigma_c)$ depends on the Weibull exponent m (2) and is normally different from the critical percolation probability $p_c = 0.592746$ of the square lattice. The equality $P(\sigma_c) = p_c$ is obtained for $m = 1.1132$, hence, for physically relevant values $m \geq 2$ used in simulations, the system is below p_c at complete breakdown. This picture radically changes when the short range interaction prevails. In this case, the stress transfer is limited to a neighborhood of the failed elements and there appear regions where a few isolated cracks drive the rupture of the material by growth and coalescence. The differences in the structure of clusters also explain the lack of a critical strength when N goes to infinity in models with local stress redistribution. Since in the GLS model the clusters are randomly dispersed across the entire lattice, the system can tolerate a larger amount of damage and a higher stress, whereas for LLS models a small increment of the external field may provoke a run away event ending with the macroscopic breakdown of the material. All the above numerical results suggest that the crossover between the mean field and the short range regimes occurs in the vicinity of $\gamma = 2$. Further support for the precise value of γ_c can be obtained by studying the change in the cluster structure of broken fibres. The moments of $n(s_c)$ defined as

$$m_k \equiv \int s_c^k n(s_c) ds \ , \tag{16}$$

where m_k is the kth moment , describe much of the physics associated with the breakdown process. We study these moments to quantitatively characterize the point where the crossover from mean field to short range behavior takes place. The zero moment $n_c = m_o$ is the total number of clusters in the system and is plotted in Fig. 10a as a function of the parameter γ. Figure 10b presents the variation of the first moment of the distribution m_1, which is equal to the total number of broken fibres $N_c = m_1$. It turns out that up to a certain value of the effective range of interaction γ, N_c remains constant and then it decreases fast until a second plateau seems to arise. Note that the constant value of N_c for small γ is in agreement with the value of the fraction of broken fibres just before the breakdown of the material in mean field models [33, 62]. This property clearly indicates a change in the evolution of the failure process and may serve as a criterion to determine the crossover point. However, a more abrupt change is observed in the average cluster size $\langle s_c \rangle$ as a function of γ. According to the moments description, the average cluster size is equal to the second moment of the cluster distribution divided by the total number of broken sites, i.e. $\langle s_c \rangle = m_2/m_1$. It can be seen in Fig. 10d that $\langle s_c \rangle$ has a sharp maximum at $\gamma = 2.2 \pm 0.1$, and thus the average cluster size drastically

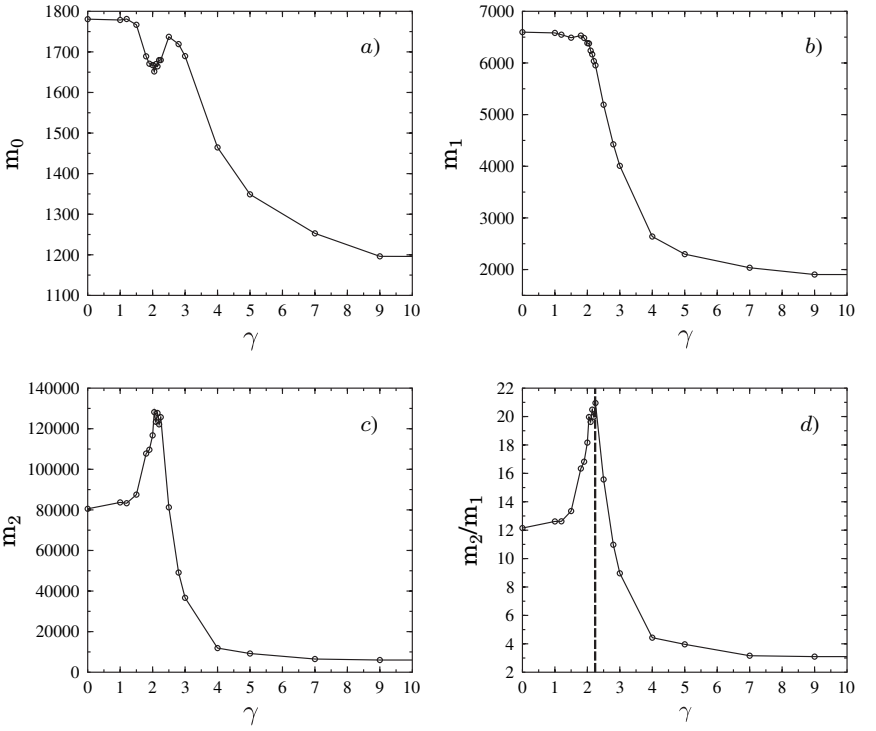

Fig. 10. Moments m_k of the clusters of broken fibres as a function of γ. The 0th and first moments are equal to the total number of clusters $n_c = m_0$ (**a**) and the total number of broken fibres $N_c = m_1$ (**b**), respectively. The average cluster size $\langle s_c \rangle$ can be determined as the ratio of the second (**c**) and first moments $\langle s_c \rangle = m_2/m_1$ (**d**)

changes at this point, which again suggests the crossover point to be in the vicinity of $\gamma_c = 2$.

5 Damage Enhanced Creep in Fibre Bundles

Under high steady stresses, materials may undergo time dependent deformation resulting in failure called creep rupture which limits their lifetime, and hence, has a high impact on their applicability in construction elements. Creep failure tests are usually performed under uniaxial tensile loading when the specimen is subjected to a constant load σ_0 and the time evolution of the damage process is followed by recording the strain ε of the specimen and the acoustic signals emitted by microscopic failure events. In order to describe the time dependent macroscopic response and finite lifetime of materials in the framework of FBMs, we extend the classical fibre bundle model presented in Sect. 2 by assuming that the fibres are viscoelastic, i.e. they exhibit time

dependent deformation under a constant external load and fail in a strain controlled manner. In the framework of the viscoelastic fibre bundle model we show by analytical and numerical calculations that there exists a critical load above which the deformation of the system monotonically increases in time resulting in global failure at a finite time t_f, while below the critical load the deformation tends to a constant value giving rise to an infinite lifetime. Our studies revealed that for global load sharing the transition between the two regimes occurs analogously to continuous phase transitions, while for local load sharing it becomes abrupt, defining two universality classes of creep rupture [25, 31, 32].

5.1 Viscoelastic Fibre Bundle

In order to capture time dependent macroscopic response in the framework of fibre bundle models, we assume that the fibres themselves are viscoelastic. For simplicity, the pure viscoelastic behavior of fibres is modelled by a Kelvin-Voigt element which consists of a spring and a dashpot in parallel and results in the constitutive equation $\sigma_0 = \beta\dot{\varepsilon} + E\varepsilon$, where σ_0 is the external load, β denotes the damping coefficient, and E is the Young modulus of fibres, respectively (see Fig. 11a).

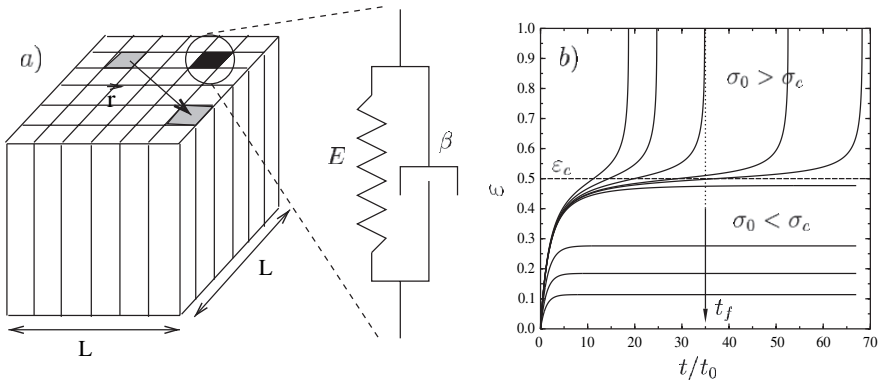

Fig. 11. (**a**) The viscoelastic fibre bundle model. Intact fibres are modelled by Kelvin-Voigt elements. (**b**) $\varepsilon(t)$ for several different values of the external load σ_0 below and above σ_c. t_0 denotes the characteristic timescale of the system $t_0 = \beta/E$

In order to capture failure in the model a strain controlled breaking criterion is imposed, i.e. a fibre fails during the time evolution of the system when its strain exceeds a breaking threshold $\varepsilon_i, i = 1, \ldots, N$ drawn from a probability distribution. For the stress transfer between fibres following fibre failure we assume that the excess load is equally shared by all the remaining intact fibres (global load sharing), which provides a satisfactory description of

load redistribution in continuous fibre reinforced composites. For the breaking thresholds of fibres a uniform distribution (1) between 0 and 1, and a Weibull distribution (2) were considered. The construction of the model is illustrated in Fig. 11a. In the framework of global load sharing most of the quantities describing the behavior of the fibre bundle can be obtained analytically. In this case the time evolution of the system under a steady external load σ_0 is described by the differential equation

$$\frac{\sigma_0}{1 - P(\varepsilon)} = \beta\dot{\varepsilon} + E\varepsilon \ , \tag{17}$$

where the viscoelastic behavior is coupled to the failure of fibres [25, 31, 32].

5.2 Macroscopic Response

The viscoelastic fibre bundle model with the equation of motion (17) can provide an adequate description of natural fibre composites like wood subjected to a constant load [15]. For the behavior of the solutions $\varepsilon(t)$ of (17), two distinct regimes can be distinguished depending on the value of the external load σ_0: when σ_0 falls below a critical value σ_c, (17) has a stationary solution ε_s, which can be obtained by setting $\dot{\varepsilon} = 0$, i.e. $\sigma_0 = E\varepsilon_s[1 - P(\varepsilon_s)]$. It means that as long as this equation can be solved for ε_s at a given external load σ_0, the solution $\varepsilon(t)$ of (17) converges to ε_s when $t \to \infty$, and the system suffers only a partial failure. However, when σ_0 exceeds the critical value σ_c no stationary solution exists, furthermore, $\dot{\varepsilon}$ remains always positive, which implies that for $\sigma_0 > \sigma_c$ the strain of the system $\varepsilon(t)$ monotonically increases until the system fails globally at a finite time t_f [25, 31, 32].

The behavior of is illustrated in Fig. 11b for several values of σ_0 below and above σ_c with uniformly distributed breaking thresholds between 0 and 1. It follows from the above argument that the critical value of the load σ_c is the static fracture strength of the bundle. The creep rupture of the viscoelastic bundle can be interpreted so that for $\sigma_0 \leq \sigma_c$ the bundle is partially damaged implying an infinite lifetime $t_f = \infty$ and the emergence of a stationary macroscopic state, while above the critical load $\sigma_0 \geq \sigma_c$ global failure occurs at a finite time t_f, but in the vicinity of σ_c the global failure is preceded by a long lived stationary state. The nature of the transition occurring at σ_c can be characterized by analyzing how the creeping system behaves when approaching the critical load both from below and above. For $\sigma_0 \leq \sigma_c$, the fibre bundle relaxes to the stationary deformation ε_s through a gradually decreasing breaking activity. It can be shown analytically that $\varepsilon(t)$ has an exponential relaxation to ε_s with a characteristic time scale τ that depends on the external load σ_0 as

$$\tau \sim (\sigma_c - \sigma_0)^{-1/2} \ , \tag{18}$$

for $\sigma_0 \leq \sigma_c$, i.e. when approaching the critical point from below the characteristic time of the relaxation to the stationary state diverges according to

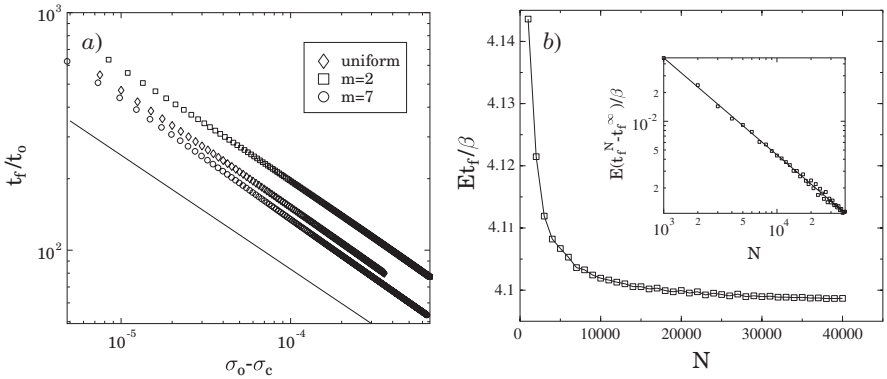

Fig. 12. (**a**) Lifetime t_f of the bundle as a function of the distance from the critical point $\sigma_0 - \sigma_c$ for three different disorder distributions, i.e. uniform distribution and Weibull distribution with $m = 2$ and $m = 7$ were considered. (**b**) t_f as a function of the number of fibres N at a fixed value of the external load σ_0. Results of computer simulations (*symbols*) are in good agreement with the analytic predictions (*solid lines*)

a universal power law with an exponent 1/2 independent on the form of the disorder distribution P.

Above the critical point the lifetime defines the characteristic time scale of the system which can be cast in the form

$$t_f \sim (\sigma_0 - \sigma_c)^{-1/2} \ , \tag{19}$$

for $\sigma_0 > \sigma_c$, so that t_f also has a power law divergence at σ_c with a universal exponent 1/2 like τ below the critical point, see Fig. 12a. Hence, for global load sharing the system exhibits scaling behavior on both sides of the critical point indicating a continuous transition at the critical load σ_c. It can also be shown analytically that fixing the external load above the critical point, the lifetime t_f of the system exhibits a universal scaling with respect to the number N of fibres of the bundle (Fig. 12b). The lifetime of finite bundles t_f^N decreases to the lifetime of the infinite bundle as $t_f^N - t_f^\infty \sim 1/N$ [25, 31].

5.3 Microscopic Damage Process

The process of fibre breaking on the micro level can easily be monitored experimentally by means of the acoustic emission techniques. Except for the primary creep regime, where a large amount of fibres break in a relatively short time, the time of individual fibre failures can be recorded with a high precision. In order to characterize the process of fibre breaking in our viscoelastic fibre bundle model, we calculated numerically the distribution f of waiting times

Δt between consecutive breaks [32]. A detailed analysis revealed that $f(\Delta t)$ shows a power law behavior on both sides of the critical point

$$f(\Delta t) \sim \Delta t^{-b} \tag{20}$$

[32]. The value of the exponent b is different on the two sides of the critical point, i.e. $b \approx 1.5$ and $b \approx 2.0$ were measured below and above the critical load; however, b proved to be independent of the disorder distribution of fibres, see Fig. 13.

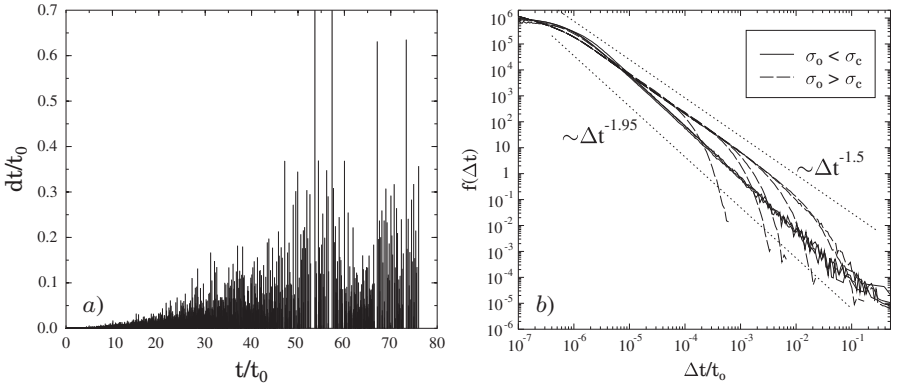

Fig. 13. (**a**) Representative example of waiting times Δt between consecutive fibre breakings for a load $\sigma_0 < \sigma_c$ plotted at the time t of breakings. (**b**) Distribution f of Δt below and above the critical load. Simulation results are presented for 10^7 fibres with uniformly distributed threshold values between 0 and 1

5.4 Universality Classes of Creep Rupture

In order to clarify the effect of the range of load sharing on damage enhanced creep, we carried out computer simulations applying the variable range of load sharing approach presented in Sect. 4 in the viscoelastic fibre bundle model (see also Fig. 11a for explanation). Simulation were carried out varying the exponent γ of the load transfer function (14) in a broad range. Computer simulations revealed that the behavior described above for global load sharing prevails in the range $0 \leq \gamma < \gamma_c$, where the value of γ_c turned to be the same as the one determined in Sect. 4 for dry fibre bundles. For $\gamma \geq \gamma_c$ the interaction of fibres becomes localized which results in an abrupt failure of the viscoelastic fibre bundle above the critical load $\sigma_0 > \sigma_c$, i.e. when σ_0 exceeds σ_c the lifetime of the bundle suddenly jumps to a finite value without any scaling behavior. It is interesting to note, however, that the power law distribution of waiting times (20) prevails for localized load sharing. The value of the exponent b below the critical load $\sigma_0 < \sigma_c$ is always $b \approx 2.0$ independent

of the effective range of load redistribution γ, while for $\sigma_0 > \sigma_c$ the exponent b increases from $\approx$1.5 to $\approx$2.0 with increasing γ [32].

6 Failure of Glued Interfaces of Solid Blocks

Solid blocks are often joined together by welding or glueing of the interfaces which are expected to sustain various types of external loads. Besides welded joints, glued interfaces of solids play a crucial role in fibre reinforced composites where fibres are embedded in a matrix material. The properties of the fibre-matrix interface are controlled by the fabrication process of the composite and have an important effect on the mechanical performance of the system.

The classical setup of fibre bundle models have recently been applied to study the failure of glued interfaces when the external load is applied perpendicular to the interface of a rigid and a compliant block [4]. It was found that the compliance of one of the solid blocks introduces stress localization and results in a fractal structure of the failed glue just before macroscopic breakdown [4]. Glued interfaces can be teared apart by applying the external load locally at one of the ending point of the interface. Such loading conditions have also been studied in the framework of FBMs considering two stiff plates [29] and also the combination of a stiff plate and a compliant one [13, 14, 60].

In all the above studies, the external load resulted in a stretching deformation of material elements of the interface so that the classical fibre bundle model discussed in Sect. 2 provided an adequate framework for the theoretical description of the failure process. However, under shear loading more complex deformation states of material elements can arise leading to a more complex degradation process, which cannot be captured by FBMs. We propose a novel approach to the shear failure of glued interfaces by extending the classical fibre bundle model to model interfacial failure [58].

6.1 The Beam Model of Interface Failure Under Shear

In our model the interface is discretized in terms of elastic beams which can be elongated and bent when exposed to shear load, see Fig. 14. The beams are assumed to have identical geometrical extensions (length l and width d) and linearly elastic behavior characterized by the Young modulus E. In order to capture the failure of the interface, the beams are assumed to break when their deformation exceeds a certain threshold value. Under shear loading of the interface, beams suffer stretching and bending deformation resulting in two modes of breaking. The stretching and bending deformation of beams can be expressed in terms of a single variable, i.e. longitudinal strain, which enables us to map the interface model to the simpler fibre bundle models. The two breaking modes can be considered to be independent or combined in the form of a von Mises type breaking criterion. The strength of beams is characterized

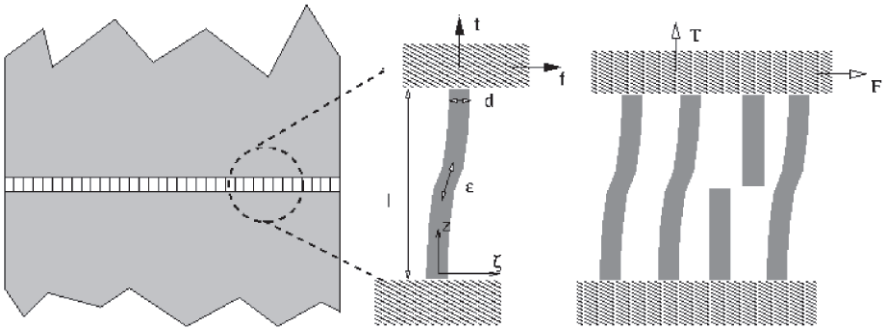

Fig. 14. Illustration of the model construction. The sheared interface is discretized in terms of beams (*left*), which suffer stretching and bending deformation (*middle*) and fail due to the two deformation modes (*right*)

by the two threshold values of stretching and bending a beam can withstand. The breaking thresholds are assumed to be randomly distributed variables of the joint probability distribution. The randomness of the breaking thresholds is supposed to represent the disorder of the interface material. After breaking of a beam the excess load has to be redistributed over the remaining intact elements. Coupling to the rigid blocks ensures that all the beams have the same deformation giving rise to global load sharing, i.e. the load is equally shared by all the elements, stress concentration in the vicinity of failed beams cannot occur.

6.2 Constitutive Behavior

Breaking of the beam is caused by two breaking modes, i.e. stretching and bending which can be either independent or coupled by an empirical breaking criterion. Assuming that the two breaking modes are independent, a beam breaks if either the longitudinal stress t or the bending moment m exceeds the corresponding breaking threshold, see Fig. 14. Since the longitudinal stress t and the bending moment m acting on a beam can easily be expressed as functions of the longitudinal deformation ε, the breaking conditions can be formulated in a transparent way in terms of ε. To describe the relative importance of the breaking modes, we assign to each beam two breaking thresholds $\varepsilon_1^i, \varepsilon_2^i$, $i = 1, \ldots, N$, where N denotes the number of beams. The threshold values ε_1 and ε_2 are randomly distributed according to a joint probability density function $p(\varepsilon_1, \varepsilon_2)$ between lower and upper bounds $\varepsilon_1^{\min}, \varepsilon_1^{\max}$ and $\varepsilon_2^{\min}, \varepsilon_2^{\max}$, respectively. The density function needs to obey the normalization condition

$$\int_{\varepsilon_2^{\min}}^{\varepsilon_2^{\max}} d\,\varepsilon_2 \int_{\varepsilon_1^{\min}}^{\varepsilon_1^{\max}} d\,\varepsilon_1\; p(\varepsilon_1, \varepsilon_2) = 1\;. \tag{21}$$

First, we provide a general formulation of the failure of a bundle of beams. We allow for two independent breaking modes of a beam that are functions f and g of the longitudinal deformation ε. Later on this case will be called the *OR* breaking rule. A single beam breaks if either its stretching or bending deformation exceed the respective breaking threshold ε_1 or ε_2, i.e. failure occurs if

$$\frac{f(\varepsilon)}{\varepsilon_1} \geq 1 \,, \quad \text{or} \tag{22}$$

$$\frac{g(\varepsilon)}{\varepsilon_2} \geq 1 \,, \tag{23}$$

where (22, 23) describe the stretching and bending breaking modes, respectively. The failure functions $f(\varepsilon)$ and $g(\varepsilon)$ can be determined from the elasticity equations of beams, but in general the only restriction for them is that they have to be monotonous. For our specific case of sheared beams they take the form

$$f(\varepsilon) = \varepsilon \,, \quad g(\varepsilon) = a\sqrt{\varepsilon} \,, \tag{24}$$

where a is a constant and the value of the Young modulus E is set to 1. In the plane of breaking thresholds each point $(\varepsilon_1, \varepsilon_2)$ represents a beam. For each value of ε those beams which survived the externally imposed deformation are situated in the area $f(\varepsilon) \leq \varepsilon_1 \leq \varepsilon_1^{\max}$ and $g(\varepsilon) \leq \varepsilon_2 \leq \varepsilon_2^{\max}$, as it is illustrated in Fig. 15a. The constitutive behavior of the interface can be obtained by integrating the load of single beams over the intact ones in the plane of breaking thresholds in Fig. 15a. For the *OR* criterion one gets

$$\sigma = \varepsilon \int_{g(\varepsilon)}^{\varepsilon_2^{\max}} d\,\varepsilon_2 \int_{f(\varepsilon)}^{\varepsilon_1^{\max}} d\,\varepsilon_1 \; p(\varepsilon_1, \varepsilon_2) \,. \tag{25}$$

Assuming the thresholds of the two breaking modes to be independently distributed, the disorder distribution factorizes $p(\varepsilon_1, \varepsilon_2) = p_1(\varepsilon_1)p_2(\varepsilon_2)$ and $\sigma(\varepsilon)$ takes the simple form

$$\sigma = \varepsilon[1 - P_1(f(\varepsilon))][1 - P_2(g(\varepsilon))] \,. \tag{26}$$

The terms $1 - P_1(f(\varepsilon))$ and $1 - P_2(g(\varepsilon))$ provide the fraction of beams failed under the stretching and bending breaking modes, respectively.

When the two breaking modes are coupled by a von Mises type breaking criterion, a single beam breaks if its strain ε fulfils the condition

$$\left(\frac{f(\varepsilon)}{\varepsilon_1}\right)^2 + \frac{g(\varepsilon)}{\varepsilon_2} \geq 1 \,. \tag{27}$$

This algebraic condition can be geometrically represented as it is illustrated in Fig. 15a. In this case the constitutive integral

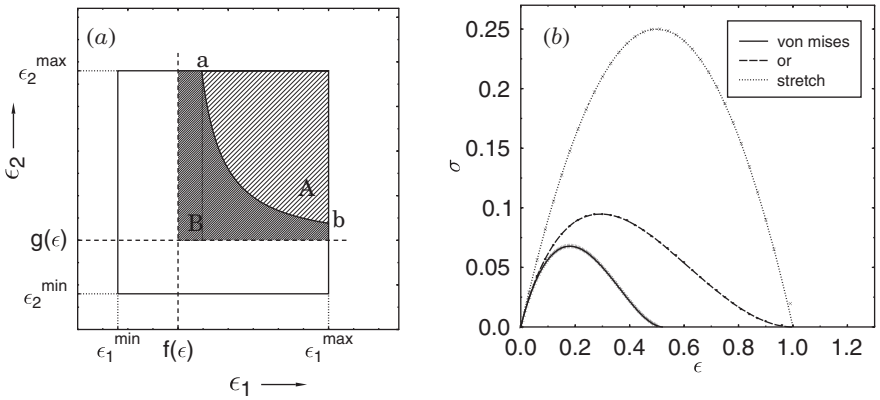

Fig. 15. (**a**) The plane of breaking thresholds. Fibres which are intact at a deformation ε fall in the rectangle bounded by $f(\varepsilon)$, $g(\varepsilon)$ and the maximum values of the two thresholds $\varepsilon_1^{\max}$, $\varepsilon_2^{\max}$ for the OR criterion (area $A + B$), and in the area bounded by the curve connecting a and b and the maximum thresholds for the von Mises type criterion (area A), respectively. The fibres which break due to the coupling of the two breaking modes in the von Mises criterion fall in area B. (**b**) Comparison of the constitutive curves of a simple dry fibre bundle and of the beam model with different breaking criteria using uniformly distributed breaking thresholds

$$\sigma = \epsilon \int_a^{\varepsilon_1^{\max}} d\varepsilon_1 \int_{\tilde{\varepsilon}_2(\varepsilon_1,\varepsilon)}^{\varepsilon_2^{\max}} d\varepsilon_2 \, p(\varepsilon_1, \varepsilon_2) \tag{28}$$

cannot be performed explicitly with the integration limit $\tilde{\varepsilon}_2(\varepsilon_1, \varepsilon) = \varepsilon_1^2 g(\varepsilon)/(\varepsilon_1^2 - f^2(\varepsilon))$ in general so that $\sigma(\varepsilon)$ cannot be obtained in a closed analytic form. The constitutive curves obtained with the OR and von Mises breaking criteria are illustrated in Fig. 15b for the specific case of a uniform distribution between $\varepsilon_1^{\min} = \varepsilon_2^{\min} = 0$ and $\varepsilon_1^{\max} = \varepsilon_2^{\max} = 1$, i.e., $P_1(\varepsilon) = \varepsilon$ and $P_2(\varepsilon) = \varepsilon$.

It follows from the structure of (26) and can be seen in Fig. 15b that the existence of two breaking modes leads to a reduction of the strength of the material, both the critical stress σ_c and strain ε_c take smaller values compared to the case of a single breaking mode applied in simple fibre bundle models [5, 12, 24, 26, 28, 37, 52, 62]. The coupling of the two breaking modes by the von Mises form (27) gives rise to further reduction of the interface strength. Note that due to the non-linearity of (27) also the functional form of $\sigma(\varepsilon)$ changes.

6.3 Simulation Techniques

Based on the above equations analytic results can only be obtained for the simplest forms of disorder like the uniform distribution. In order to determine the behavior of the system for complicated disorder distributions and explore

the microscopic failure process of the sheared interface, it is necessary to work out a computer simulation technique. For the simulations we consider an ensemble of N beams arranged on a square lattice (see Fig. 1). Two breaking thresholds $\varepsilon_1^i, \varepsilon_2^i$ are assigned to each beam i ($i = 1, \ldots, N$) of the bundle from the joint probability distribution $p(\epsilon_1, \epsilon_2)$. For the OR breaking rule, the failure of a beam is caused either by stretching or bending depending on which one of the conditions (22, 23) is fulfilled at a lower value of the external load. In this way an effective breaking threshold ϵ_c^i can be defined for the beams as

$$\epsilon_c^i = \min(f^{-1}(\varepsilon_1^i), g^{-1}(\varepsilon_2^i)), \qquad i = 1, \ldots, N \,, \tag{29}$$

where f^{-1} and g^{-1} denote the inverse of f, g, respectively. A beam i breaks during the loading process of the interface when the load on it exceeds its effective breaking threshold ϵ_c^i. For the case of the von Mises type breaking criterion (27), the effective breaking threshold ϵ_c^i of beam i can be obtained as the solution of the algebraic equation

$$\left(\frac{f(\epsilon_c^i)}{\epsilon_1^i}\right)^2 + \frac{g(\epsilon_c^i)}{\epsilon_2^i} = 1, \qquad i = 1, \ldots, N \,. \tag{30}$$

In the case of global load sharing, the load and deformation of beams is everywhere the same along the interface, which implies that beams break in increasing order of their effective breaking thresholds. In the simulation, after determining ϵ_c^i for each beam, they are sorted in increasing order. Quasi-static loading of the beam bundle is performed by increasing the external load to break only a single element. Due to the subsequent load redistribution on the intact beams, the failure of a beam may trigger an avalanche of breaking beams. This process has to be iterated until the avalanche stops, or leads to catastrophic failure at the critical stress and strain.

In Fig. 15b the analytic results on the constitutive behavior obtained with uniform distribution of the breaking thresholds are compared to the corresponding results of computer simulations. As a reference, we also plotted the constitutive behavior of a bundle of fibres where the fibres fail solely due to simple stretching (i.e., DFBM) [5, 12, 24, 26, 28, 37, 52, 62]. It can be seen in the figure that the simulation results are in perfect agreement with the analytical predictions. It is important to note that the presence of two breaking modes substantially reduces the critical stress σ_c and strain ε_c (σ_c and ε_c are the value of the maximum of the constitutive curves) with respect to the case when failure of elements occurs solely under stretching [5, 12, 24, 26, 28, 37, 52, 62]. Since one of the failure functions is non-linear, the shape of the constitutive curve also changes, especially in the post-peak regime. The coupling of the two breaking modes in the form of the von Mises criterion gives rise to further reduction of the strength of the interface, see Fig. 15b.

6.4 Microscopic Damage Process

During the quasi-static loading process of an interface, avalanches of simultaneously failing beams occur. Inside an avalanche, however, the beams can break solely under one of the breaking modes when the OR criterion is considered, or the breaking can be dominated by one of the breaking modes in the coupled case of the von Mises type criterion. In order to study the effect of the disorder distribution of beams on the relative importance of the two breaking modes and on the progressive failure of the interface, we considered independently distributed breaking thresholds both with a Weibull distribution of exponents m_1 and m_2, and scale parameters λ_1 and λ_2 for the stretching and bending modes, respectively. It can be seen in Fig. 16a that increasing λ_2 of the bending mode, the beams become more resistant against bending so that the stretching mode starts to dominate the breaking of beams, which is indicated by the increasing fraction of stretching failure. In the limiting case of $\lambda_2 \gg \lambda_1$ the beams solely break under stretching. It is interesting to note that varying the relative importance of the two failure modes gives also rise to a change of the macroscopic constitutive behavior of the system. Shifting the strength distributions of beams, the functional form of the constitutive behavior remains the same, however, the value of the critical stress and strain vary in a relatively broad range. Varying the amount of disorder in the breaking thresholds, i.e. the Weibull exponents, has a similar strong effect on the macroscopic response of the system, see Fig. 16b. Applying the von Mises

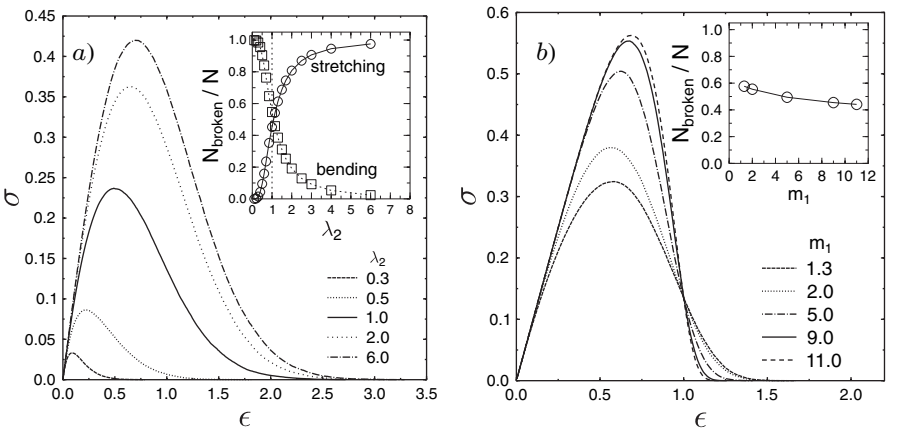

Fig. 16. (**a**) Constitutive behavior of a bundle of $N = 90000$ beams using the OR criterion for different values of the scale parameter λ_2 of the bending mode. The other parameters were fixed $m_1 = m_2 = 2.0$ and $\lambda_1 = 1.0$. Inset: fraction of beams broken under the two breaking modes. (**b**) Constitutive behavior of the same bundle changing the Weibull exponent m_1 of the stretching mode with $\lambda_1 = \lambda_2 = 1.0$ and $m_2 = 2.0$. Inset: the fraction of beams broken under the bending mode

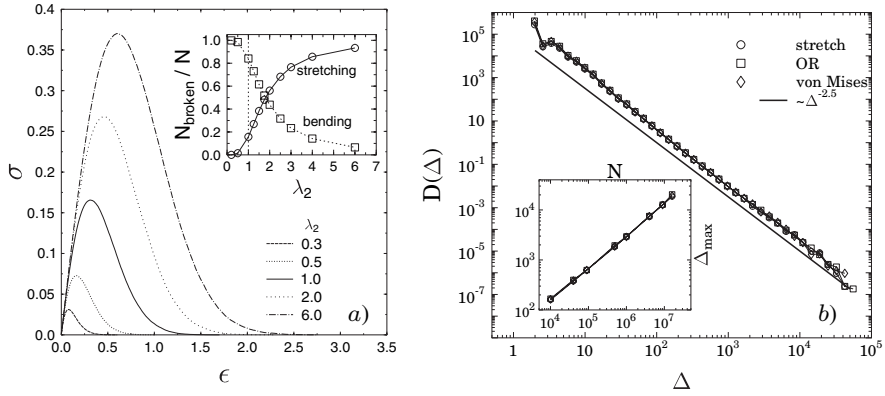

Fig. 17. (**a**) Constitutive behavior of the interface applying the von Mises breaking criterion at different values of the scale parameter λ_2 of the bending threshold. (**b**) Comparison of the avalanche size distribution for the classical DFBM, the OR and the von Mises type breaking criteria. The inset shows that the size of largest avalanche $\Delta_{\max}$ is proportional to the size of the bundle N

breaking criterion, the microscopic and macroscopic response of the interface show similar behavior (Fig. 17a). Our careful numerical analysis of the microscopic failure process of the interface revealed that the size of avalanches of simultaneously failing beams under stress controlled loading of the interface has a power law distribution (Fig. 17b). The exponent of the power law proved to be 5/2; it is equal to the mean field exponent characterizing the distribution of burst in simple fibre bundle models [28].

7 Discussion and Outlook

We presented an overview of recent extensions of the classical fibre bundle model in order to provide a more realistic description of the fracture and breakdown of disordered materials. We gradually improved the model by generalizing the damage law, constitutive behavior, deformation state and the way of interaction of the fibres. Analytical calculations and computer simulations have been carried out to explore the macroscopic response and the microscopic damage process of the extended model, which was then confronted with the classical FBM intensively studied in the literature.

Recently, several applications of the extended fibre bundle models have been proposed in a broad range of breakdown phenomena. The continuous damage fibre bundle model with the gradual degradation of fibre strength proved to adequately describe the relevant damage mechanism of various types of materials. CDFBM was successfully applied to understand the strength and fracture mechanism of nacre [43, 44], where even a quantitative comparison

to experimental findings was possible. CDFBMs have also been considered to describe node breaking failures in scale free networks [38], and it has been further generalized considering time dependent fibre strength [34, 35].

An interesting study of the viscoelastic fibre bundle model was performed in [39, 40] where the model was further improved considering a more realistic time dependent response of single fibres instead of Kelvin-Voigt elements [40]. The authors carried out creep rupture experiments of fibre composites with randomly oriented short fibres and found a quantitative agreement of the model predictions and experimental results on the macro and micro behavior of the system [39]. The careful analyzes of the accumulation of damage in the viscoelastic fibre bundle model also helps to construct forecasting methods of the imminent macroscopic failure [64].

Based on the variable range of load sharing provided by the load transfer function (14), interesting results have recently been achieved on the analogy of damage and fracture to phase transitions and critical phenomena. Analyzing FBMs on scale free networks showed that besides the range of interaction also the structure of connectivity of the bundle is crucial to determine the universality class of the fracture transition [10]. Apart from fibre reinforced composites, short range interaction of fibres proved to be important also for the mechanical behavior and rupture of biological tissues [27].

Acknowledgements

This work was supported by the Collaborative Research Center SFB 381 and by the NATO Grant PST.CLG.977311. H.J. Herrmann is grateful for the Max Planck Prize. F. Kun acknowledges financial support of the Research Contracts NKFP 3A-043/2004, OTKA M041537, T049209 and of the György Békésy Foundation of the Hungarian Academy of Sciences. The authors are grateful to Y. Moreno for valuable discussions.

References

1. M.P. Allen and D.J. Tildesley, Editors, *Computer Simulation of Liquids*, Oxford University Press, Oxford (1984).
2. J.V. Andersen, D. Sornette, and K. Leung, Tricritical Behaviour in Rupture Induced by Disorder, Phys. Rev. Lett., **78** 2140–2143 (1997).
3. G.G. Batrouni and A. Hansen, Fracture in three-dimensional fuse networks, Phys. Rev. Lett., **80** 325 (1998).
4. G.G. Batrouni, A. Hansen, and J. Schmittbuhl, Heterogeneous interfacial failure between two elastic blocks, Phys. Rev. E, **65** 036126 (2002).
5. P. Bhattacharyya, S. Pradhan, and B.K. Chakrabarti, Phase transition in fibre bundle models with recursive dynamics, Phys. Rev. E, **67**(14) 046122 (2003).
6. B.K. Chakrabarti and L.G. Benguigui, *Statistical Physics of Fracture and Breakdown in Disordered Systems*, Oxford University Press, Oxford (1997).

7. B.D. Coleman, Time dependence of mechanical breakdown phenomena, J. Appl. Phys., **27** 862 (1956).
8. W.A. Curtin, The "tough" to brittle transition in brittle matrix composites, J. Mech. Phys. Solids, **41** 217 (1993).
9. W.A. Curtin, Size Scaling of Strength in Heterogeneous Materials, Phys. Rev. Lett., **80** 1445–1448 (1998).
10. D.-H. Kim, B.J. Kim, and H. Jeong, Universality class of the fibre bundle model on complex networks, Phys. Rev. Lett., **94** 025501 (2005).
11. Ravá da Silveira, An introduction to breakdown phenomena in disordered systems, Am. J. Phys., **67** 1177 (1999).
12. H.E. Daniels, The statistical theory of the strength of bundles of threads-I, Proc. R. Soc. London A, **183** 405–435 (1945).
13. A. Delaplace, S. Roux, and G. Pijaudier-Cabot, Damage cascade in a softening interface, Int. J. Solids Struct., **36** 1403–1426 (1999).
14. A. Delaplace, S. Roux, and G. Pijaudier-Cabot, Avalanche Statistics of Interface Crack Propagation in Fibre Bundle Model: Characterization of Cohesive Crack, J. Eng. Mech., **127** 646–652 (2001).
15. G. Dill-Langer, R.C. Hidalgo, F. Kun, Y. Moreno, S. Aicher, and H.J. Herrmann, Size dependency of tension strength in natural fibre composites, Physica A, **325** 547–560 (2003).
16. A.G. Evans and F.W. Zok, The physics and mechanics of fibre-reinforced brittle matrix composites, Journal of Materials Science, **29** 3857–3896 (1994).
17. J.B. Gómez, D. Iñiguez, and A.F. Pacheco, Solvable Fracture Model with Local Load Transfer, Phys. Rev. Lett., **71** 380 (1993).
18. A. Hansen and P.C. Hemmer, Burst Avalanches in Bundles of Fibres: Local Versus Global Load-Sharing, Phys. Lett. A, **184** 394–396 (1994).
19. A. Hansen and S. Roux, Statistical toolbox for damage and fracture. In D. Krajcinovic and J. van Mier, Editors, *Damage and Fracture of Disordered Materials*, number 410 in CISM Courses and Lectures, Chap. 2, pp. 17–101. Springer Verlag (2000).
20. D.G. Harlow and S.L. Phoenix, The Chain-of-Bundles Probability Model For the Strength of Fibrous Materials i: Analysis and Conjectures, J. Composite Materials, **12** 195 (1978).
21. D.G. Harlow and S.L. Phoenix, The Chain-of-Bundles Probability Model for the Strength of Fibrous Materials ii: A Numerical Study of Convergence, J. Composite Materials, **12** 314 (1978).
22. P.C. Hemmer and A. Hansen, The Distribution of Simultaneous Fibre Failures in Fibre Bundles, J. Appl. Mech., **59** 909–914 (1992).
23. H.J. Herrmann and S. Roux, Editors, *Statistical models for the fracture of disordered media*, Random materials and processes, Elsevier, Amsterdam (1990).
24. R.C. Hidalgo, F. Kun, and H.J. Herrmann, Bursts in a fibre bundle model with continuous damage, Phys. Rev. E, **64**(6) 066122 (2001).
25. R.C. Hidalgo, F. Kun, and H.J. Herrmann, Creep rupture of viscoelastic fibre bundles, Phys. Rev. E, **65** 032502 (2002).
26. R.C. Hidalgo, Y. Moreno, F. Kun, and H. J. Herrmann, Fracture model with variable range of interaction, Phys. Rev. E, **65** 046148 (2002).
27. B.J. Kim, Phase transitions in the modified fibre bundle model, Europhys. Letts., **66** 819 (2004).
28. M. Kloster, A. Hansen, and P.C. Hemmer, Burst avalanches in solvable models of fibrous materials, Phys. Rev. E, **56** 2615–2625 (1997).

29. J. Knudsen and A.R. Massih, Breakdown of disordered media by surface loads, Phys. Rev. E, **72** 036129 (2005).
30. F. Kun and H.J. Herrmann, Damage development under gradual loading of composites, Journal of Materials Science, **35** 4685 (2000).
31. F. Kun, R.C. Hidalgo, H.J. Herrmann, and K.F. Pal, Scaling laws of creep rupture of fibre bundles, Phys. Rev. E, **67**(6) 061802 (2003).
32. F. Kun, Y. Moreno, R.C. Hidalgo, and H.J. Herrmann, Creep rupture has two universality classes, Europhys. Lett., **63**(3) 347–353 (2003).
33. F. Kun, S. Zapperi, and H. J. Herrmann, Damage in fibre bundle models, Eur. Phys. J. B, **17** 269 (2000).
34. L. Moral, J.B. Gomez, and Y. Moreno, Exact numerical solution for a time-dependent fibre-bundle model with continuous damage, J. Phys. A-Math. Gen., **34** 9983 (2001).
35. L. Moral, Y. Moreno, J.B. Gomez, and A.F. Pacheco, Time dependence of breakdown in a global fibre-bundle model with continuous damage, Phys. Rev. E, **63** 066106 (2001).
36. Y. Moreno, J.B. Gómez, and A.F. Pacheco, Self-organized criticality in a fibre-bundle-type model, Physica A, **274** 400 (1999).
37. Y. Moreno, J.B. Gomez, and A.F. Pacheco, Fracture and second-order phase transitions, Phys. Rev. Lett., **85**(14) 2865–2868 (2000).
38. Y. Moreno, J.B. Gomez, and A.F. Pacheco, Instability of scale-free networks under node-breaking avalanches, Eur. Phys. Lett., **58** 630 (2002).
39. H. Nechad, A. Helmstetter, R. El Guerjouma, and D. Sornette, Andrade and critical time to failure laws in fibre-matrix composites: Experiments and model, J. Mech. Phys. Solids, **53** 1099 (2005).
40. H. Nechad, A. Helmstetter, R. El Guerjouma, and D. Sornette, Creep ruptures in heterogeneous materials, Phys. Rev. Lett., **94** 045501 (2005).
41. W.I. Newman and A.M. Gabrielov, Failure of hierarchical distributions of fibre bundles, International Journal of Fracture, **50** 1–14 (1991).
42. W.I. Newman, D.L. Turcotte, and A.M. Gabrielov, log-periodic behavior of a hierarchical failure model with applications to precursory seismic activation, Phys. Rev. E, **52** 4827 (1995).
43. P.K. Nukala and S. Simunovic, A continuous damage random thresholds model for simulating the fracture behavior of nacre, Biomaterials, **26** 6087 (2005).
44. P.K. Nukala and S.Simunovic, Statistical physics models for nacre fracture simulation, Phys. Rev. E, **72** 041919 (2005).
45. P.V.V. Nukala, S. Simunovic, and S. Zapperi, Percolation and localization in the random fuse model, J. Stat. Mech: Theor. Exp., p. P08001 (2004).
46. F.T. Peires, Tensile tests for cotton yarns. v.-'the weakest link', theorems on the strength of long composite specimens, J. Textile Inst., **17** T355–368 (1926).
47. S.L. Phoenix and I.J. Beyerlein, Statistical Strength Theory for Fibrous Composite Materials, volume 1 of *Comprehensive Composite Materials*, Sect. 1.19, pages 1–81. Pergamon, Elsevier Science, N. Y. (2000).
48. S.L. Phoenix, M. Ibnabdeljalil, and C.-Y. Hui, Int. J. Solids Structures, **34** 545 (1997).
49. S.L. Phoenix and I.J. Beyerlein, Statistical Strength Theory for Fibrous Composite Materials, In A. Kelly and C. Zweben, Editors, *Comprehensive Composite Materials*, Vol. 1, Sect. 1.19. Pergamon, Elsevier Science, New York (2000).
50. S.L. Phoenix and R. Raj, Scalings in fracture probabilities for a brittle matrix fibre composite, Acta metall. mater., **40** 2813 (1992).

51. S. Pradhan and B.K. Chakrabarti, Precursors of catastrophe in the Bak-Tang-Wiesenfeld, Manna, and random-fibre-bundle models of failure, Phys. Rev. E, **65** 016113 (2002).
52. S. Pradhan and B.K. Chakrabarti, Failure due to fatigue in fibre bundles and solids, Phys. Rev. E, **67**(14) 046124 (2003).
53. S. Pradhan and B. K. Chakrabarti, Failure properties of fibre bundle models, Int. J. Mod. Phys. B, **17** 5565–5581 (2003).
54. S. Pradhan, A. Hansen, and P.C. Hemmer, Crossover behavior in burst avalanches: Signature of imminent failure, Phys. Rev. Lett., **95** 125501 (2005).
55. S. Pradhan, A. Hansen, and P.C. Hemmer, Crossover behavior in burst avalanches: Signature of imminent failure, Phys. Rev. Lett., **95** 125501 (2005).
56. S. Pradhan and A. Hansen, Failure properties of loaded fibre bundles having a lower cutoff in fibre threshold distribution, Phys. Rev. E, **72** 026111 (2005).
57. S.R. Pride and R. Toussaint, Thermodynamics of fibre bundles, Physica A, **312** 159–171 (2002).
58. F. Raischel, F. Kun, and H.J. Herrmann, Simple beam model for the shear failure of interfaces, Phys. Rev. E, **72** 046126 (2005).
59. S. Roux, Thermally activated breakdown in the fibre-bundle model, Phys. Rev. E, **62** 6164 (2000).
60. S. Roux, A. Delaplace, and G. Pijaudier-Cabot, Damage at heterogeneous interfaces, Physica A, **270** 35–41 (1999).
61. R. Scorretti, S. Cilibreto, and A Guarino, Disorder enhances the effect of thermal of thermal noise in the fibre bundle model, Europhys. Lett., **55** 626–632 (2001).
62. D. Sornette, Elasticity and failure of a set of elements loaded in parallel, J. Phys. A, **22** L243–L250 (1989).
63. D. Sornette, Mean-field solution of a block-spring model of earthquakes, J. Phys. I. France, **2** 2089 (1992).
64. D. Sornette. Statistical physics of rupture in heterogeneous media. In S. Yip, editor, *Handbook of Materials Modeling*, Sect. 4.4. Springer Science and Business Media (2005).
65. D. Sornette and J.V. Andersen, Scaling with respect to disorder in time-to-failure, Eur. Phys. J. B, **1** 353 (1998).
66. R. Toussaint and S.R. Pride, Interacting damage models mapped onto Ising and percolation models, Phys. Rev. E, **71** 046127 (2005).
67. D.L. Turcotte and M.T. Glasscoe, A damage model for the continuum rheology of the upper continental crust, Tectonophysics, **383** 71–80 (2004).
68. E. Vives and A. Planes, Avalanches in a fluctuationless first-order phase transition in a random-bond ising model, Phys. Rev. B, **50** 3839 (1994).
69. S. Zapperi, P. Ray, H.E. Stanley, and A. Vespignani, First-Order Transition in the Breakdown of Disordered Media, Phys. Rev. Lett., **78** 1408 (1997).
70. S. Zapperi, P. Ray, H.E. Stanley, and A. Vespignani, Analysis of damage clusters in fracture processes, Physica A, **270** 57 (1999).
71. S. Zapperi, P. Ray, H.E. Stanley, and A. Vespignani, Avalanches in breakdown and fracture processes, Phys. Rev. E, **59** 5049 (1999).
72. S. Zapperi, A. Vespignani, and H.E. Stanley, Plasticity and avalanche behaviour in microfracturing phenomena, Nature, **388** 658 (1997).